Preprint, 2019

Published 2 December 2019
International Journal of Modern Physics A
Vol. 34, No. 36 (2019) 1942041 (16 pages)
DOI: 10.1142/S0217751X19420417

Also FERMILAB-PUB-19-092-PPD,
GM2-doc-19832

Computation of the Main and Fringe Fields for the Electrostatic Quadrupoles of the Muon *g*-2 Storage Ring*

Eremey Valetov†, Martin Berz, Kyoko Makino
Department of Physics and Astronomy, Michigan State University
East Lansing, Michigan 48824, the United States of America

Received Day Month Year
Revised Day Month Year

We developed a highly accurate and fully Maxwellian conformal mapping method for calculation of main fields of electrostatic particle optical elements. A remarkable advantage of this method is the possibility of rapid recalculations with geometric asymmetries and mispowered plates. We used this conformal mapping method to calculate the multipole terms of the high voltage quadrupoles in the storage ring of the Muon *g*-2 Experiment (FNAL-E-0989). Next, we demonstrate that an effect where the observed tunes correspond to a voltage that is about 4 % higher compared to the voltage to which the Muon *g*-2 quadrupoles are set is explained by the conceptual and quantitative differences between the beam optics quadrupole voltage and the quadrupole voltage at the plates. Completing the methodological framework for field computations, we present a method for extracting multipole strength falloffs of a particle optical element from a set of Fourier mode falloffs. We calculated the quadrupole strength falloff and its effective field boundary (EFB) for the Muon *g*-2 quadrupole, which has explained the experimentally measured tunes, while simple estimates based on a linear model exhibited discrepancies up to 2 %.

Keywords: Muon g-2; anomalous magnetic dipole moment; storage rings; electrostatic quadrupoles; main field; multipole expansion; fringe field; effective field boundary; tunes; plate misalignments; mispowered plates; voltages; differential algebra; conformal mapping methods.

PACS numbers: 41.20.Cv, 29.20.Dh, 14.60.Ef, 13.40.Em, 02.30.Mv, 02.60.Cb

1. Introduction

Methods for measurement of the anomalous magnetic dipole moment (MDM) and the electric dipole moment (EDM) using a storage ring rely on electrostatic particle optical elements, including the Muon *g*-2 Experiment's storage ring at Fermi National Accelerator Laboratory (FNAL). Accordingly, it is necessary to accurately

*Fermilab report FERMILAB-PUB-19-092-PPD.

†Email: evaletov@fnal.gov. ORCID: 0000-0003-4341-0379. Presently also affiliated with the Physics Department, Lancaster University, Bailrigg, Lancaster LA1 4YW, UK, as well as with the Cockcroft Institute of Accelerator Science and Technology, Daresbury International Science Park, Daresbury, Warrington WA4 4AD, UK.

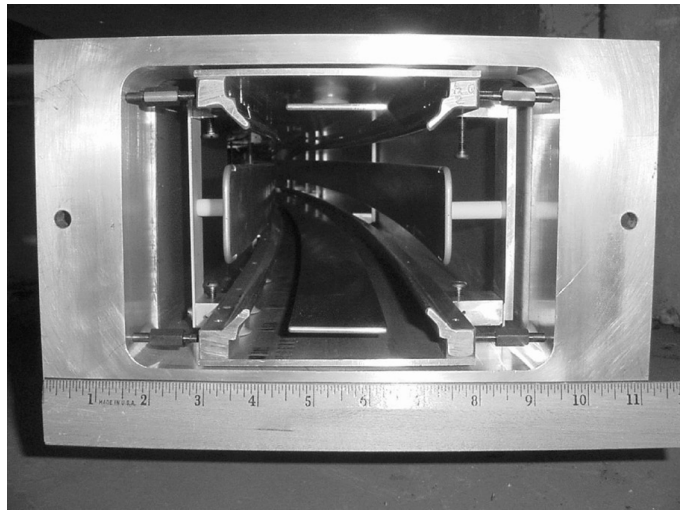

Fig. 1. Photograph of the Muon g-2 quadrupole, comprising quadrupole plates, trolley rails, and a vacuum chamber. (Reprinted from Nucl. Instr. Meth. Phys. Res. A, Vol. 503, Yannis K. Semertzidis et al., The Brookhaven Muon g-2 Storage Ring High Voltage Quadrupoles, Page No. 476, Copyright 2003, with permission from Elsevier.)

model main and fringe fields of electrostatic elements, in particular because energy conservation in an electrostatic field requires an accurate integration of the equations of motion along the particle trajectory, whereas in case of the magnetic field energy conservation is trivial.

In this research, we address the representation and field calculation problem by considering the specific case of the electrostatic quadrupoles[1] of the Muon g-2 Experiment's storage ring ("Muon g-2 quadrupoles"; see photograph in Fig. 1), to the general geometric and electrostatic properties of which we refer in singular as the Muon g-2 quadrupole.

We developed a conformal mapping method for calculation of main fields of electrostatic particle optical elements. Conformal mapping methods provide an analytic formula defining a fully Maxwellian map to a polygonal model of the element, where curves can be approximated using linear interpolation. Our model of the main field of the Muon g-2 quadrupole allows rapid recalculations with geometric asymmetries and mispowered plates, the latter being useful, *inter alia*, for simulations of RF scraping and the effects of damaged quadrupole resistors.

We used the multipole terms of the Muon g-2 quadrupole calculated using conformal mapping methods to propose an alternative explanation for an effect where when a voltage is set on the plates of a Muon g-2 quadrupole, the observed tunes correspond to a voltage that is about 4 % higher than the set voltage. This effect was named the "oomph" effect,[2] and the term "oomph" was used since within the Muon g-2 collaboration. (One previously hypothesized explanation of this effect had been that the quadrupole plates were all 49.11 mm from the reference orbit instead

of the nominal design aperture 50 mm, which, due to the quadratic dependence of the quad strength on the length scale, resulted in an increase of the quadrupole strength by about 4 %.) From here on forward we will also use the term "oomph" for this effect. Oomph is necessary to match muon loss simulations with the observed loss data, as well as the muon loss peaks with the betatron resonance lines.

For fields with a longitudinal dependence such as fringe fields, Fourier analysis at one radius is insufficient for multipole strength calculation; however, multipole strengths can be extracted from Fourier modes calculated at multiple radii. For the fringe field of the Muon g-2 quadrupole, we calculated the field map using a BEM solver. We calculated the falloffs of the Fourier modes for the field of the quadrupole and extracted the falloff of the quadrupole strength, which, with consideration of our conclusions regarding the oomph effect, resulted in an excellent agreement of calculated tunes with experimentally measured tunes.

This paper presents and discusses methods for computation of main and fringe electrostatic fields and applies them to the Muon g-2 quadrupole, and it additionally explains the oomph effect, where electrostatic quadrupoles have apparently higher voltages than set in the control room.

2. Conformal Mapping Methods

We used conformal mapping methods[3] for calculation of the main field on the Muon g-2 quadrupole, which is described in this paper, as well as to calculate fringe fields of electrostatic deflectors.[3] A conformal mapping (or conformal map) is a transformation $f : \mathbb{C} \to \mathbb{C}$ that is locally angle preserving. A conformal mapping satisfies Cauchy–Riemann equations and, therefore, its real and imaginary parts satisfy Laplace's equation: $\Delta\Re(f) = 0$ and $\Delta\Im(f) = 0$. Conformal mappings automatically provide the electrostatic potential in cases where the electrostatic element's geometry can be represented by a polygon, possibly with some vertices at the infinity. The domain of a conformal mapping is called the canonical domain, and the image of a conformal mapping is called the physical domain. A Schwarz–Christoffel mapping is a conformal mapping from the upper half-plane as the canonical domain to the interior of a polygon as the physical domain.

The electrostatic potential for a cross section or a longitudinal section modeled by a generalized polygon may be found by obtaining a conformal mapping f from a suitable canonical domain to the polygon. A bi-infinite strip is a suitable canonical domain if the polygon comprises two groups of consecutive sides characterized by the same constant Dirichlet boundary condition, with two constant values in total. A rectangular part of a bi-infinite strip is a suitable canonical domain when the physical domain is a logical (or generalized) quadrilateral.

If the solution of the Laplace equation in the canonical domain is ϕ, the solution of the Laplace equation in the physical domain is $\varphi = \phi \circ f^{-1}$. In practice, the electrostatic potential is usually the appropriately selected, shifted, and scaled real or imaginary part of f^{-1}.

The solution for the electrostatic potential obtained this way is fully Maxwellian in the sense that the analytic formula for f or f' results in the solution for the potential satisfying the Laplace equation.

As described in,[4,5] inverse conformal mapping $g = f^{-1}$ may be obtained by

(i) solving the equation

$$f\left(g\left(w\right)\right) - w = 0 \tag{1}$$

using the Newton–Raphson or another numerical method; or

(ii) solving the ODE[3]

$$\frac{dg\left(w\right)}{dw} = \frac{1}{f'\left(g\left(w\right)\right)}, \quad g\left(w_0\right) = z_0. \tag{2}$$

3. Main Field of the Muon *g*-2 Electrostatic Quadrupole

The main field of an electrostatic element such as the Muon g-2 collaboration quadrupole can be obtained using the following general method:[3]

(i) Calculate the electrostatic potential using conformal mapping methods with one plate at 1 V and the other Dirichlet boundary conditions (the remaining plates, the rectangular enclosure, and the trolley rails) of 0 V.
(ii) Apply plate distance errors as perturbations to four copies of the potential, each copy corresponding to one plate at 1 V and the other Dirichlet boundary conditions of 0 V.
(iii) Apply appropriate rotations to these four copies of the potential, scale the copies (e.g., by $\pm 2.4 \times 10^4$ or with mispowered values), and use their superposition.

We considered two polygonal models of the cross section: (1) the nominal case with symmetric voltages and no geometric asymmetries ("symmetric model"), and (2) the general case of mispowered plates and geometric asymmetries ("nonsymmetric model"). In the former case, we simplified the polygonal model using the four-fold rotational symmetry and the four mirror symmetries, as Fig. 2 shows. The conformal mapping theory for physical domains as n-connected regions for $n \geq 2$ is quite challenging or restricted (see, e.g., Ref. 6 and Ref. 4) compared to simply-connected regions. We approximated the cross-sectional geometry in the nonsymmetric model by a simply-connected region shown in Fig. 3 by adding rectangular connecting bars between the rectangular enclosure and the four plates, which were placed in the middle of the back side of each plate to minimize their impact on the multipole terms.

The physical device uses connecting rods, which are made from a dielectric material, to hold the plates in position. These connecting rods can be seen in Fig. 1. For application of the conformal mapping method in the nonsymmetric model case, we used rectangular connecting bars as a mathematical measure, which were modeled as von Neumann boundary conditions with equipotential lines normal to the boundary. Modifying or adding any boundary condition in the polygonal model changes the equipotential lines and the multipole terms of the potential. However, placing the

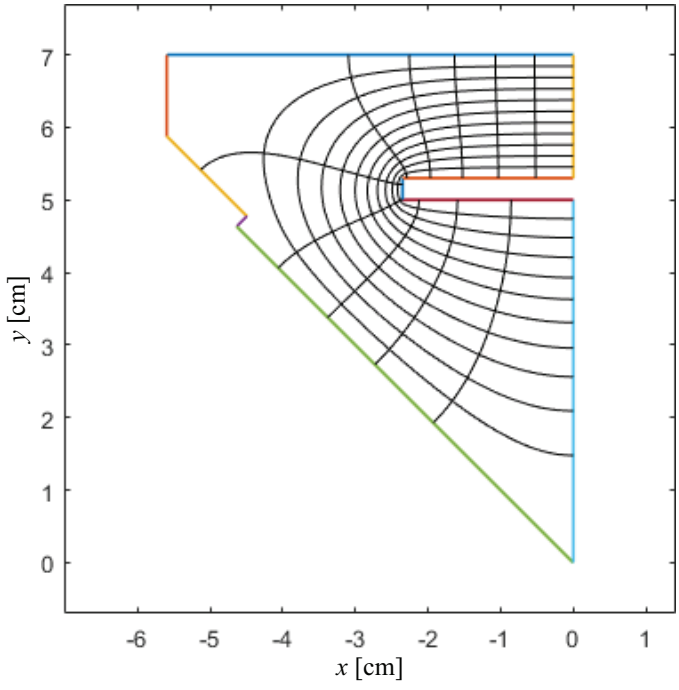

Fig. 2. The polygonal model of 1/8th part of cross section of the Muon g-2 quadrupole in the symmetric model case, obtained from the full cross section using the four-fold rotational symmetry and the four mirror symmetries.

connecting bars in the vertical and horizontal midplanes behind the plates, where the equipotential lines are almost parallel to the nearby plate and vacuum chamber wall, minimizes the effect of the bars on the multipole terms. Indeed, if the equipotential lines were perfectly parallel, or if the connecting bars were infinitely thin and the quadrupole had a full four-fold symmetry, the connecting bars would have no effect. The connecting bars were made as thin as possible while avoiding conformal mapping algorithm convergence problems due to the crowding phenomenon.

In both symmetric and nonsymmetric cases, considering that two constant Dirichlet boundary conditions are interposed by two von Neumann boundary conditions, forming a logical quadrilateral, we used a conformal mapping from a rectangular part of a bi-infinite strip. The derivative of the conformal map f from the canonical domain to the physical domain was[4]

$$f'(z) = c\,\mathrm{cn}(z|m)\,\mathrm{dn}(z|m)\prod_{j=1}^{n}\left(\mathrm{sn}(z|m) - \mathrm{sn}\left(x_j + iy_j|m\right)\right)^{\alpha_j - 1},$$

where sn, cn, and dn are the Jacobi elliptic functions,[7] the number of vertices n and angles $\pi\alpha$ are parameters of the polygonal model, and the parameters x, y, m, and c were found using the *SC Toolbox*.[8]

Before proceeding further, we briefly introduce the method of differential algebras (DA),[9] which is used for various calculations discussed in this paper. Among

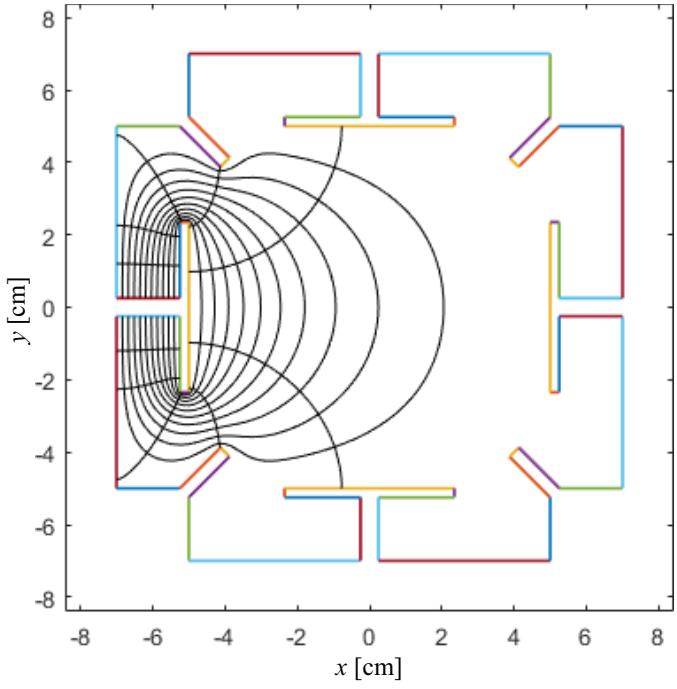

Fig. 3. The polygonal model of the cross section of the Muon g-2 quadrupole in nonsymmetric model case.

many, one of the advantages of DA computations is that Taylor series expansions can be produced automatically for a highly complex analytic function by substituting its comprising functions with their DA values. Another advantageous technique is the DA fixed-point algorithm, e.g., for the inversion of a Taylor series expansion, that completes in finitely many steps. The code *COSY INFINITY*[10] has an efficient implementation of multivariate differential algebra (DA).[9] For the purpose of cross-checking of various computations, we also used *Mathematica* to compute some Taylor series expansions. In our CPU time tests[3] *COSY INFINITY*'s DA implementation was significantly faster than respective calculations in *Mathematica* by two to three orders of magnitude.

Knowing the analytic expression for a derivative f' of a conformal mapping f and the constant part

$$g_0 = \mathrm{cons}\,(g\,(0)) \in \mathbb{C}$$

of the DA value of $g = f^{-1}$, i.e. the DA value's scalar part, at the origin $w = 0$, we can obtain the DA inverse $g\,(0)$ at the origin as

$$g\,(0) = g_0 + \left(\partial^{-1} f'\,(g_0)\right)^{-1}.$$

Symmetric model In the symmetric model case, the derivative f' of the conformal mapping has a branch point at the preimage of the origin, which corresponds to the reference orbit. This presents certain difficulties in the analysis. For example,

it is not possible to obtain the electrostatic potential multipole terms by obtaining f via a Taylor series expansion of f' and then calculating the inverse series. The same applies to the calculation of DA values of f at point $z = g_0$.

In view of this, for the symmetric model case, we obtained the multipole expansion of the electrostatic potential for the Muon g-2 quadrupole up to order 24 in the form

$$\varphi(r,\theta) = \frac{A_0}{2} + \sum_{j=1}^{24} r^j \left(A_j \cos(j\theta) + B_j \sin(j\theta)\right) + O\left(r^{25}\right)$$

by solving the restriction of the ODE from Eq. 2 to the vertical edge of the polygonal model, using the solution as a boundary condition in solving the Cauchy–Riemann PDE in *Mathematica*, and performing Fourier analysis.

We also calculated the multipole expansion in *MATLAB* in the symmetric model case up to order 24 by computing the inverse values of the conformal mapping object `f` at an equidistant discretization of a circle of radius `R` into $N = 1001$ arc intervals of length $\triangle t = 2\pi \mathtt{R}/N$ as

$$u = \left(\mathtt{f}^{-1}\left(\mathtt{R}\cos(j\triangle t), \mathtt{R}\sin(j\triangle t)\right)\right)_{j=0}^{N-1},$$

taking the discrete Fourier transform (DFT) of the electrostatic potential φ around the circle, and obtaining the Fourier modes using the Hermitian symmetry.

Nonsymmetric model For the nonsymmetric model case, we obtained the multipole expansion up to order 24 using the DA inverse of the conformal mapping in *COSY INFINITY* and *Mathematica*, as well as using Fourier analysis applied to its conventional inverse in *MATLAB*. In particular, we produced a *COSY INFINITY* program called `mterms`, as well as its variant written in *Python*, which calculates the multipole terms of the Muon g-2 quadrupole for a given set of mispowered plates and plate misalignments.

Fig. 4 shows a heatmap plot of the multipole expansion of the electrostatic potential to order 24. Fig. 5 shows multipole strengths higher than the quadrupole strength, i.e. the multipole expansion from order 3 to order 24. Because the contributions of these higher multipole strengths in the quadrupole are relatively small within the aperture, Fig. 5 uses a contour plot with a logarithmic contour scale to visualize the magnitude levels.

Our *a posteriori* error analysis indicates that the DA method is accurate. This application of the conformal mapping method was near its limit in terms of the complexity of geometry due to the crowding phenomenon,[11] where crowding refers to a close collocation of preimages of the polygon vertices. However, the method can be expanded to significantly more complex geometries using the cross ratios of the Delaunay triangulation (CRDT) algorithm.[3,4,12,13] The conformal mapping method has the advantage of an analytic, fully Maxwellian formula and allows rapid recalculations with adjustments to the geometry and mispowered plates,[3] as opposed to BEM and FEM solvers such as *COULOMB*[14] and *Opera-3d*.[15]

The multipole terms we calculated for the Muon g-2 quadrupole were used to study the effects of an unpowered plate and for RF scraping studies. In the next

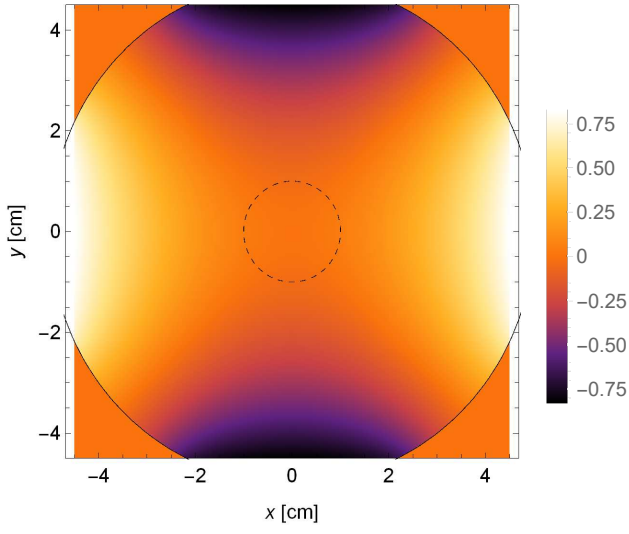

Fig. 4. A heatmap plot of the multipole expansion of the electrostatic potential to order 24 in the nonsymmetric model case. This multipole expansion was obtained using the DA inverse in *COSY INFINITY*; the DA inverse in *Mathematica* and Fourier analysis in *MATLAB* produced visually identical results. Calculations were performed for unitless voltages ± 1 on the plates. The plot is valid within the aperture radius $R_{\mathrm{a}} = 50$ mm, denoted by the solid black circle.

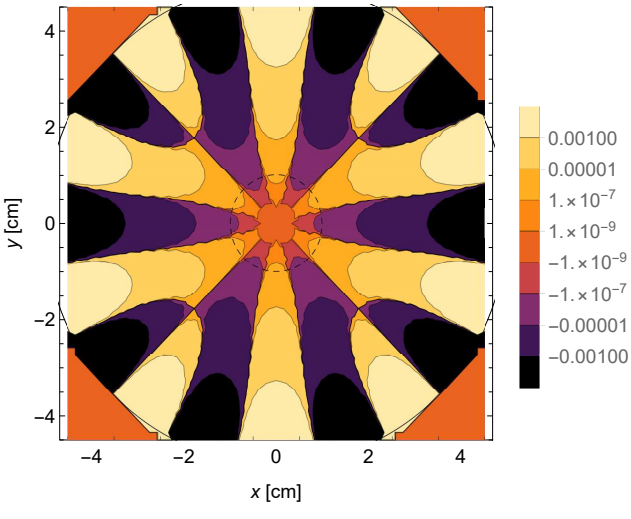

Fig. 5. A contour plot showing the multipole expansion of the electrostatic potential without the quadrupole strength in the nonsymmetric model case, i.e. orders 3 to 24. The contributions of these higher multipole strengths in the quadrupole are relatively small within the aperture, and logarithmic scale contours are used to visualize the magnitude levels. This multipole expansion was obtained using the DA inverse in *COSY INFINITY*. The scaling of the multipole expansion from Fig. 4 was preserved. The plot is valid within the aperture radius $R_{\mathrm{a}} = 50$ mm, denoted by the solid black circle.

section, we use these multipole terms to explain the oomph effect. The multipole terms were also used to study the effect of damaged resistors with affected RC time constants on beam dynamics variables such as the beta function, tunes, and coherent betatron oscillation frequencies in the Muon g-2 storage ring.

4. The Oomph Effect and Two Quad Voltages

In this section, we analyze the oomph effect in the context of the main field of the quadrupoles. The explanation for the oomph effect that we will propose, however, due to its nature, is applicable to both main and fringe fields. We note that the term "quadrupole voltage" refers to two different things: (1) the voltage that is set on the quadrupole plates by the control room, and (2) the beam optics quadrupole voltage that is directly relevant to calculating the tune.

The tune is subject to the quadrupole voltage

$$V_{2,2} = M_{2,2} R_{\mathrm{a}}^2,$$

where R_{a} is the aperture radius $R_{\mathrm{a}} = 50\,\mathrm{mm}$ and $M_{2,2}$ is the quadrupole strength in the multipole expansion[9]

$$\varphi(s, r, \theta) = \sum_{k=0}^{+\infty} \sum_{l=0}^{+\infty} M_{k,l}(s) \cos(l\theta + \theta_{k,l})\, r^k. \tag{3}$$

In this multipole expansion, $\varphi(s, r, \theta)$ is the electrostatic potential, where s is the longitudinal and (r, θ) are the polar transversal particle optical coordinates.

On the other hand, the voltage on the plate is the sum of the contributions of all multipole voltages $V_{l,l}$, which can be calculated using the multipole expansion in Eq. 3. For the sake of illustration, considering the scaling properties of electrostatics, we examined the case of the plates set to $V_{\mathrm{plate}} = 1\,\mathrm{V}$.

We express the beam optics multipole voltages of the main field of the Muon g-2 quadrupole as normal multipole voltages v_n and skew multipole voltages w_n in the expansion

$$\varphi(r, \theta) = \frac{v_0}{2} + \sum_{n=1}^{+\infty} \left(\frac{r}{R_{\mathrm{a}}}\right)^n (v_n \cos(n\theta) + w_n \sin(n\theta)). \tag{4}$$

We considered three cases "Semertzidis *et al.*", "Wu", and "Valetov" of multipole strengths of the Muon g-2 quadrupole. The multipole strengths were independently calculated by Semertzidis *et al*[1] and Wanwei Wu[16] using Opera-3d's FEM solver in their respective cases. The multipole strengths in our case "Valetov" were calculated using conformal mapping methods as described in Sec 3. The model used for calculation of Valetov multipole strengths has a full four-fold symmetry, and it would be sufficient to calculate the plate voltage for one plate. Semertzidis *et al.* multipole strengths have a nearly four-fold symmetry, which can also be seen from the cross-sectional geometry model in Fig. 18 of Ref. 1. On the other hand, Wu multipole strengths are based on full 3D calculations including the curved longitudinal axis, resulting in no four-fold symmetry.

Case "Semertzidis *et al.*" We obtained the multipole voltages (v_n, w_n) by scaling the multipole normal and skew strengths (A_n, B_n) from the values in Table 5 of Ref. 1 at $R_{\text{ref}} = 45\,\text{mm}$ and the plate voltage $V_{\text{s}} = 24\,\text{kV}$ as

$$(v_n, w_n) = (A_n, B_n)\,\frac{V_{\text{s}}}{V_{\text{plate}}}\left(\frac{R_{\text{a}}}{R_{\text{ref}}}\right)^n,$$

where $V_{\text{plate}} = 1\,\text{V}$.

Case "Wu" We performed Fourier analysis at reference radius $R_{\text{ref}} = 45\,\text{mm}$ for the Muon g-2 quadrupole main field data obtained by Wanwei Wu based on full 3D *Opera-3d* FEM.[16] We calculated the multipole voltages (v_n, w_n) by scaling the resulting multipole strengths (A_n, B_n) to the aperture radius R_{a}.

Case "Valetov" We calculated the multipole voltages (v_n, w_n) by scaling to the aperture radius R_{a} from the multipole strengths (A_n, B_n) that we obtained for the Muon g-2 quadrupole in the symmetric model case (see Sec. 3) using Fourier analysis performed using *MATLAB*,[3] at reference radius $R_{\text{ref}} = 45\,\text{mm}$.

As an accuracy cross check, for each of the sets of beam optics multipole voltages, we calculated the plate voltages as sums of multipole voltage contributions. The calculations were performed using Eq. 4 at the aperture radius R_{a} and polar angles $\theta = 0°$, $90°$, $180°$, and $270°$, corresponding to the middle of each quadrupole plate. Table 1 shows the results of these calculations. The accuracies in terms of the magnitudes of plate voltages approximating 1V were 4×10^{-5}V for Valetov multipole voltages, 1.6×10^{-3}V for Wu voltages, and 2.5×10^{-3}V for Semertzidis *et al.* voltages.

All three models and the corresponding voltage calculations show the quadrupole voltage is $(V_{2,2} - V_{\text{plate}})/V_{\text{plate}} = 4\,\%$ higher than the plate voltage magnitude: the multipole voltages add up to the correct plate voltage of 1 V, but the quadrupole voltage is about 1.04 V. It is worth to note that the multipoles maintain a constant voltage across the longitudinal quadrupole plates, which are not equipotential lines of a pure quadrupole.

The 4 % effect (1) quantitatively explains the shift of the peaks in *COSY INFINITY* muon loss simulations relative to the observed effects,[17] and it (2) quantitatively allows to reproduce the measured tunes, as Table 2 shows.

Table 1. Plate voltages of the Muon g-2 quadrupole calculated from multipole voltages obtained in cases Semertzidis *et al.*, Wu, and Valetov at polar angles $\theta = 0°$, $90°$, $180°$, and $270°$. The values in this table show how well the plate voltages ±1 V that were used to obtain these multipole voltages are approximated.

θ	Semertzidis *et al.*	Wu	Valetov
$0°$	0.99772	1.00159	0.99996
$90°$	−0.99652	−1.00002	−0.99996
$180°$	0.99772	1.00064	0.99996
$270°$	−0.99652	−1.00000	−0.99996

5. Fringe Field of the Muon *g*-2 Electrostatic Quadrupole

In the fringe field of an electrostatic particle optical element, the expansion of the electrostatic field, from including the dependence of the field on the longitudinal coordinate s, takes the general Taylor–Fourier form[3]

$$\varphi(r,\theta,s)=\sum_{k=0}^{+\infty}\sum_{l=0}^{+\infty}M_{k,l}(s)\cos\left(l\theta+\theta_{k,l}\right)r^{k}.$$

Multipole terms $M_{k,l}(s)$ vanish for $k<l$ and $k=l+1,l+3,\ldots$ in the general case.[9] We compare it with the Fourier expansion of the electrostatic potential

$$\varphi(r,\theta,s)=\frac{a_0(r,s)}{2}+\sum_{l=0}^{+\infty}a_l(r,s)\cos(l\theta+\theta_l),$$

where we assume $a_0(r,s)$ to be zero, considering the gauge invariance of the electrostatic potential. Thus, for a set of radii r_j for $j=1,2,\ldots,N$,

$$a_l(r_j)=\sum_{m=0}^{+\infty}M_{l+2m,l}r_j^{l+2m}, \tag{5}$$

and we can extract an approximation of the $2l$-pole strength $M_{l,l}$ from Fourier modes a_l by solving a matrix equation.[18]

We developed a *Python* program called *STEP File Generator* (or `stepfg`). This program produces 3D STEP[19] (ISO 10303-242) files from polygonal models specified by vertices. Compared to performing this process manually in CAD software, our software has workflow efficiency advantages. The output file in the STEP format can be used in many general 3D programs, including BEM and FEM field solvers. Using the *STEP File Generator*, we effectively extruded a polygonal model of a 90° section of the full cross section of the Muon g-2 quadrupole. Because the curvature radius $R=711.2$ cm is relatively large compared to the half-aperture $d=5$ cm, the approximation of a straight reference orbit is quite accurate for the purpose of calculating the fringe field.

The electrostatic potential was calculated by Helmut Soltner using *COULOMB*'s BEM field solver[14] and our input data at a grid-point set of coordinates with radii

$$r=1.8,2.1,2.4,2.7,3.0\,\text{cm} \tag{6}$$

and longitudinal coordinates with the discretization size ranging from $\triangle z=0.625$cm generally to $\triangle z=0.078$cm near the edge of the quadrupole, where the field falloff is the steepest. We note that the conformal mapping method we presented in Sec. 3 is applicable to 2D fields and not applicable to 3D fields such as fringe fields of electrostatic quadrupoles.

From the field data using *COULOMB*, we calculated the Fourier mode falloffs using the DFT and the Hermitian symmetry at the above set of radii. Next, we extracted the quadrupole strength falloff for the Muon g-2 quadrupole using Eq. 5. From the quadrupole strength falloff, we calculated the effective field boundary (EFB) $z_{\text{EFB}}=1.2195$ cm. We also fitted an Enge function model using the Levenberg–Marquardt Gauss–Newton method to the falloff of the quadrupole

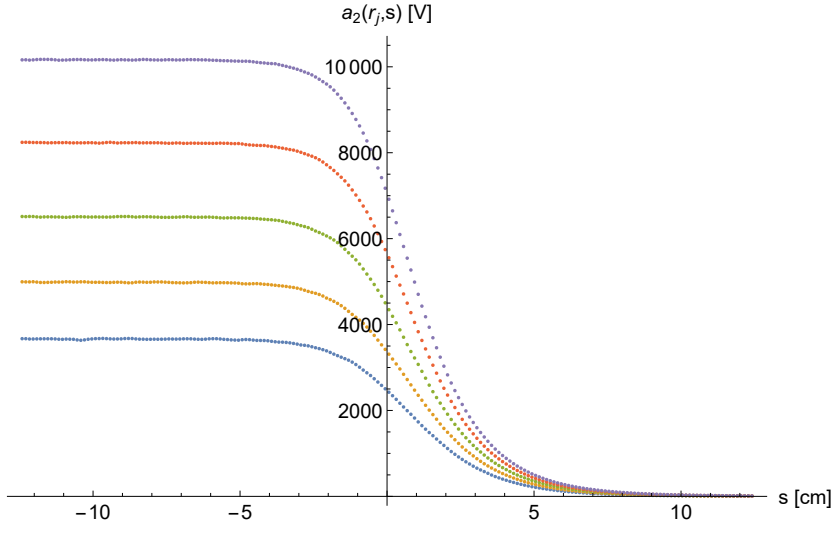

Fig. 6. Falloffs of 2nd order Fourier modes $a_2\,(r_j)$ calculated at radii $r = 1.8, 2.1, 2.4, 2.7, 3.0$ cm from Wu field data.[16] Curves with larger magnitudes correspond to larger radii.

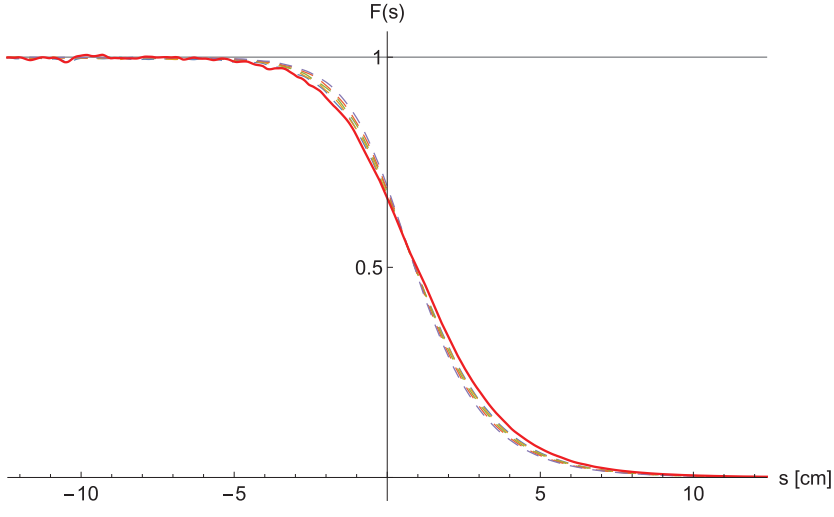

Fig. 7. The Fourier modes $a_2\,(r_j)$ (five thin dashed curves) alone fall off more quickly than the quadrupole strength $M_{2,2}$ (solid curve); all curves are scaled to 1 well inside the quadrupole. This is because the second derivative of $M_{2,2}\,(s)$ is negative in the fringe field at $s \lesssim 0$ cm and positive at $s \gtrsim 0$ cm, impacting the additional terms based on the second derivative of $M_{2,2}$ in Eq. 5.

strength,[3] because Enge function coefficients are the necessary input parameters to model fringe fields in *COSY INFINITY*[10] for beam dynamics computations.

For a comparison, we applied the same multipole strength extraction method to the electrostatic field data obtained by Wanwei Wu[16] using *Opera-3d*'s FEM

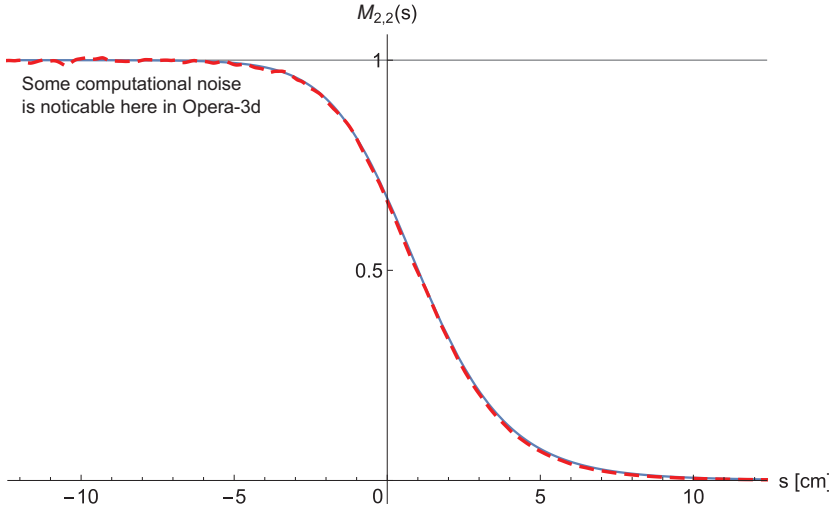

Fig. 8. The falloff of the multipole term $M_{2,2}$ based on Soltner–Valetov field data ($z_{\mathrm{EFB}} = 1.2195\,\mathrm{cm}$; thin solid curve) and based on Wu field data[16] ($z_{\mathrm{EFB}} = 1.1233\,\mathrm{cm}$; thick dashed curve), calculated by us in both cases. The difference 0.0962 cm in the EFBs is 2 % compared to the aperture radius 5 cm.

field solver. Wu field data accounts for the curvature of the reference orbit. To apply the multipole strength extraction method, we interpolated the data to obtain field data at the set of radii of Eq. 6, because Wu field data is for a rectangular grid in each transversal plane. Fig. 6 shows the resulting Fourier mode falloffs. In Fig. 7, we compare these Fourier modes with the extracted quadrupole strength $M_{2,2}$. Additionally, we fitted the multipole expansion to the raw field data in each cross section and obtained similar results. The field falloffs and the EFBs obtained from Soltner–Valetov and Wu field data are in good agreement as shown in Fig. 8.

6. Comparison of Computed and Measured Tunes

In the previous sections, we have discussed a series of efficient and accurate methods of constructing faithful models of the main and fringe fields of the electrostatic quadrupole of the Muon g-2 storage ring. Our discussions started from the conformal mapping method to calculate the multipole terms of the main field not only for symmetric voltage cases with symmetric geometries but also for general cases with mispowered plates or asymmetric geometries, and we utilized the DA method in the process. Since electrostatic fields fall off very slowly compared to magnetic fields, it is particularly important to model the fringe field both for the falloff profile and for identifying the EFB, and we calculated the fringe field falloff of the quadrupole strength using the 3D field data obtained via *COULOMB*'s BEM solver. The computed multipole strengths for the main field and for the fringe field falloffs are compared with those obtained based on *Opera-3d*'s FEM field data, resulting in a good agreement, and particularly the main field demonstrating much

Table 2. Tunes of the Muon g-2 storage ring computed (1) by us using a simple linear model and (2) by David Tarazona for a detailed nonlinear model accounting for the higher order multipole terms, the fringe field falloffs, EFBs, and also the magnetic field imperfection.[17] They are compared with tunes obtained by Antoine Chapelain using fiber harp experimental measurements (preliminary),[16] where the data errors are 0.04 % (13 kV) to 0.05 % (20.5 kV) for ν_x and 0.2 % (20.5 kV) to 0.3 % (13 kV) for ν_y. Relative differences $\Delta\nu_{x,y}/\nu_{x,y}$ of the computed tunes to the measured tunes are listed. The magnetic field imperfection in the nonlinear model contributed 0.01 % to ν_x and −0.1 % to ν_y compared to the equivalent nonlinear model without it.

Horizontal Tunes	13 kV	15 kV	19 kV	20.5 kV
Linear model ν_x	0.9624	0.9565	0.9446	0.9401
Linear model $\Delta\nu_x/\nu_x$	0.129 %	0.149 %	0.212 %	0.211 %
Nonlinear model ν_x	0.9609	0.9547	0.9424	0.9377
Nonlinear model $\Delta\nu_x/\nu_x$	−0.033 %	−0.037 %	−0.023 %	−0.041 %
Vertical Tunes	**13 kV**	**15 kV**	**19 kV**	**20.5 kV**
Linear model ν_y	0.2715	0.2916	0.3282	0.3410
Linear model $\Delta\nu_y/\nu_y$	−1.734 %	−1.769 %	−2.222 %	−2.026 %
Nonlinear model ν_y	0.2783	0.2990	0.3369	0.3500
Nonlinear model $\Delta\nu_y/\nu_y$	0.715 %	0.724 %	0.343 %	0.575 %

higher accuracy compared to the latter.

In the DA based framework of *COSY INFINITY*,[10] faithful values of main field multipole strengths, the Enge function coefficients, and the EFBs for the fringe fields are necessary parameters to model an element such as the Muon g-2 electrostatic quadrupole to conduct nonlinear beam dynamics simulations for a system such as the Muon g-2 storage ring. One of the first questions in beam dynamics calculations of a storage ring is to obtain tune values, and so it is for the Muon g-2 storage ring. Typically at the very early stage of a system setup, linear tunes are estimated based on the design values of field parameters. Horizontal and vertical tune values based on a linear model of the Muon g-2 electrostatic quadrupole are listed in Table 2, where the quadrupole main field strength $M_{2,2}$ alone is taken into account, which directly relates to the plate voltage without any higher multipole terms, fringe field falloffs, or EFBs. With the parameters obtained through the methods and the calculations discussed in this paper, we can now describe the system more realistically than a linear model. Using the computational mechanism in *COSY INFINITY*, we computed tunes with various levels of details. Table 2 lists tune values computed using one of the most detailed nonlinear models of the Muon g-2 storage ring, which includes the consideration of the magnetic field imperfection.[17]

As expected, we observed discrepancies between the linear model tunes and the nonlinear model tunes as seen in Table 2. In the linear model case, they were about −2 % for vertical tunes ν_y and 0.1 % to 0.2 % for horizontal tunes ν_x. We compared both with the experimentally measured (preliminary) tunes,[16] and the relative differences to the measured (preliminary) values are listed in Table 2, where the nonlinear model represents much higher agreement. It is worth to note that the

relative differences for the nonlinear model are comparable to the data errors of the measured (preliminary) tunes,[16] which are noted in the table caption. The larger differences seen in the vertical tunes can be explained by the tendency of off-midplane particles to have smaller vertical tunes than the vertical tune in the midplane, and the particles in the experimental measurements have a non-zero variance of the vertical position. A quantitative analysis of this effect on vertical tunes can be performed by studying amplitude-dependent tune shifts, and regarding that we refer to Ref. 20 and an earlier study in Ref. 21.

Acknowledgments

We would like to thank Wanwei Wu for providing field data using *Opera-3d*, Antoine Chapelain for providing experimentally obtained (preliminary) tunes using fiber harp measurements, David Tarazona for providing a set of computed tune values for a detailed nonlinear model including the magnetic field imperfection, and Helmut Soltner (Forschungszentrum Jülich) for running *COULOMB* field calculations with our input data. We thank David Tarazona, William Morse, Mike Syphers, and Alexander Herrod for interesting and valuable discussions regarding the oomph effect. We acknowledge the Muon g-2 collaboration, in the context of which this research was performed. This work was supported by the U.S. Department of Energy under Contract No. DE-FG02-08ER41546. This manuscript has been authored by Fermi Research Alliance, LLC under Contract No. DE-AC02-07CH11359 with the U.S. Department of Energy, Office of Science, Office of High Energy Physics.

References

1. Y. K. Semertzidis *et al.*, *Nucl. Instrum. Methods A* **503**, 458 (2003).
2. W. Morse, Private communication.
3. E. Valetov, *Field Modeling, Symplectic Tracking, and Spin Decoherence for EDM and Muon g-2 Lattices*, PhD thesis, Fermilab report FERMILAB-THESIS-2017-21, Michigan State University (2017).
4. T. A. Driscoll and L. N. Trefethen, *Schwarz–Christoffel Mapping* (Cambridge University Press, Cambridge, UK, 2002).
5. L. N. Trefethen, *SIAM J. Sci. and Stat. Comput.* **1**, 82 (1980).
6. D. Crowdy, *Proc. R. Soc. A* **461**, 2653 (2005).
7. See mathworld.wolfram.com/JacobiEllipticFunctions.html for definitions of the Jacobi elliptic functions.
8. T. A. Driscoll, *ACM Trans. Math. Softw.* **22**, 168 (1996).
9. M. Berz, *Modern Map Methods in Particle Beam Physics* (Academic Press, San Diego, CA, 1999).
10. K. Makino and M. Berz, *Nucl. Instrum. Methods A* **558**, 346 (2006), doi:10.1016/j.nima.2005.11.109.
11. L. Banjai. Private communication.
12. T. A. Driscoll and S. A. Vavasis, *SIAM J. Sci. Comput.* **19**, 1783 (1998).
13. L. Banjai, *SIAM J. Sci. Comput.* **30**, 618 (2008).
14. INTEGRATED Engineering Software, *COULOMB* https://www.integratedsoft.com/product/coulomb/.

15. Vector Fields Limited, *OPERA-3d User Guide* (Vector Fields Limited, Oxford, England, 2004).
16. Data provided by the Muon g-2 collaboration at Fermilab.
17. D. Tarazona, M. Berz and K. Makino, *Int. J. Mod. Phys. A* (in these proceedings).
18. R. Jagasia. Private communication.
19. ISO/IEC, *IS 10303-242:2014 Industrial Automation Systems and Integration – Product Data Representation and Exchange – Part 242: Application Protocol: Managed Model-Based 3D Engineering* (International Organization for Standardization, Geneva, Switzerland, 2014).
20. A. Weisskopf, D. Tarazona and M. Berz, *Int. J. Mod. Phys. A* (in these proceedings).
21. N. M. Gelfand, Amplitude Dependence of the Tune Shift, in *Proc. of the 1987 IEEE Particle Accelerator Conference (PAC1987): Accelerator Engineering and Technology, March 16-19, 1987 Washington, D.C.*, (IEEE, New York, NY, 1987), pp. 1014–1016.